Lagrangian Analysis of the Meridional Overturning Circulation in an Idealized Ocean Basin

LUKE P. VAN ROEKEL AND TAKA ITO

Department of Atmospheric Science, Colorado State University, Fort Collins, Colorado

PATRICK T. HAERTEL

Department of Geology and Geophysics, Yale University, New Haven, Connecticut

DAVID A. RANDALL

Department of Atmospheric Science, Colorado State University, Fort Collins, Colorado

(Manuscript received 5 August 2008, in final form 23 March 2009)

ABSTRACT

The Lagrangian ocean model is used as a tool to simulate the response of the basin-scale overturning circulation to spatially variable diapycnal mixing in an idealized ocean basin. The model explicitly calculates the positions, velocities, and tracer properties of water parcels. Owing to its Lagrangian formulation, numerical diffusion is completely eliminated and water parcel pathways and water mass ages can be quantified within the framework of the discrete, advective transit time distribution. To illustrate the ventilation pathways, simulated trajectories were tracked backward in time from the interior ocean to the surface mixed layer where the water parcel was last in contact with the atmosphere. This new diagnostic has been applied to examine the response of the meridional overturning circulation to highly localized diapycnal mixing through sensitivity experiments. In particular, the focus is on three simulations: the first holds vertical diffusivity uniform; in the second, the vertical diffusivity is confined within an equatorial box; and the third simulation has a diffusivity pattern based on idealized hurricane-induced mixing. Domain-integrated deep ventilation rates and heat transport are similar between the first two cases. However, locally enhanced mixing yields about 30% younger water mass age in the tropical thermocline due to intense localized upwelling. In the third simulation, a slower ventilation rate of deep waters is found to be due to the lack of abyssal mixing. These results are interpreted using the classical theories of abyssal circulation, highlighting the strong sensitivity of the ventilation pathways to the spatial distribution of diapycnal mixing.

1. Introduction

The ocean's meridional overturning circulation (MOC) and poleward heat transport are sensitive to the rate of turbulent mixing in the interior ocean (Bryan 1987; Zhang et al. 1999; Park and Bryan 2000). Beyond the vertical diffusion of heat and tracers, diapycnal mixing can control the upwelling of deep waters and the horizontal circulations through the buoyancy and vorticity balance (Stommel and Arons 1960; Munk 1966).

Early theoretical studies derived scaling relationships between diapycnal diffusivity (κ) and intensity of the MOC based on geostrophy and vertical advective–diffusive balance (Lineikin 1955; Robinson and Stommel 1959; Welander 1986), and the theoretical scaling is further developed to include interactions with the wind-driven gyres (Samelson and Vallis 1997). These scaling relationships have been tested against numerical simulations (Hu 1996; Marotzke 1997; Zhang et al. 1999; Park and Bryan 2000). Further, these scaling relations have profound effects on the ocean biogeochemistry and carbon cycle (Ito and Follows 2003; Ito and Deutsch 2006).

Turbulent mixing in stratified fluids lifts the center of mass and requires a continuous input of mechanical energy. The ultimate origin of this energy may be surface

Corresponding author address: Luke P. Van Roekel, Dept. of Atmospheric Science, Colorado State University, 1371 Campus Delivery, Fort Collins, CO 80523-1371.
E-mail: luke@atmos.colostate.edu

DOI: 10.1175/2009JPO4110.1

winds and tidal currents (Wunsch and Ferrari 2004). Further, it has been speculated that diapycnal mixing is highly variable in both space and time (Munk and Wunsch 1998), possibly localized into a limited number of ''hot spots.'' Recent in situ measurements of turbulent mixing are beginning to resolve the spatial variability of diapycnal diffusivity. Ledwell et al. (1993) measured relatively small mixing rates in the open ocean thermocline, $O(10^{-5}\ \mathrm{m^2\ s^{-1}})$. A weaker mixing in the open ocean would require a compensating region of strong mixing in order to maintain a vigorous global MOC. Observations do lend credence to highly localized mixing. Elevated diffusivities are, indeed, observed in association with topographic features and internal wave fields (Polzin et al. 1997; Garrett 2003; Hibiya et al. 2006) and with salt fingers (Schmitt et al. 2005). Further, Sriver and Huber (2007) present evidence for hurricanes strongly influencing mixing in the tropical surface ocean.

These emerging observations pose an outstanding question on the role of highly localized diapycnal mixing in modulating the MOC and the oceanic transport of heat, carbons, and biogeochemical tracers. Numerical ocean models have been used to study the role of spatially variable mixing on the large-scale ocean circulations (e.g., Marotzke 1997; Hasumi and Suginohara 1999; Kamenkovich and Goodman 2001; Scott and Marotzke 2002; Endoh and Hibiya 2007). These modeling studies have used Eulerian ocean general circulation models (OGCMs) in which the evolution of ocean currents and tracers are calculated on Eulerian grids. In Eulerian models, however, it is difficult to fully control the rate of tracer diffusion because tracer fields can be prone to spurious diffusion (Griffies et al. 2000).

In this paper, we use the Lagrangian ocean model (LOM) as a tool to simulate the response of the basin-scale ocean circulation to the spatially variable diapycnal mixing in an idealized ocean basin. The LOM explicitly calculates the positions, velocities, and tracer properties of water parcels for the entire model domain (Haertel and Randall 2002).

There are two major advantages with Lagrangian models. First, diffusion of tracers can be controlled explicitly, which makes this model particularly suitable for the examination of ocean circulation in the limit of highly localized diffusion. Another advantage is the explicit simulation of water parcel trajectories. Alternatively, parcel trajectories are estimated in Eulerian models by placing ''floats'' in the model and advecting them with simulated flow fields. This approach can be susceptible to interpolation and advection errors, which will increase in time (Ozgökmen et al. 2000). In this study, the parcel trajectories are one of the prognostic variables and there is no need to place these floats.

To illustrate the three-dimensional pathways of water masses, we develop the discrete ''advective transit time distribution'' (aTTD) by tracing the simulated trajectories backward in time from the interior ocean to the surface mixed layer where the water parcel was last in contact with the atmosphere. The transit time distribution (TTD) measures the probability density of the transit time from the surface mixed layer to a point in the interior ocean, including the effects of complex water parcel pathways and the parameterization of subgrid-scale turbulence (Holzer and Hall 2000). The first moment of TTD is the mean age, which is a widely used diagnostic property for tracer transport. In this paper, aTTD is defined as the discrete set of the transit time for a set of water parcel trajectories from a particular water mass, which reflects the transport due to the resolved circulation. TTD and aTTD become nearly identical in the limit case where subgrid-scale diffusion is not important (e.g., ventilated thermocline).

We apply this new diagnostic to examine the response of thermohaline overturning to highly localized diapycnal mixing through sensitivity experiments using LOM configured for a single hemispheric basin. In particular, we compare three simulations: in the first, the vertical diffusivity is uniform. In the second, vertical diffusivity is confined within an equatorial region. In the final simulation, the vertical diffusivity is based on an idealized version of hurricane-induced mixing (based on Korty et al. 2008).

Our purpose is twofold: first, owing to the explicit control over diffusion in this model, we present a cleaner picture of how the circulation changes with the highly localized diapycnal mixing, including three-dimensional pathways from isopycnal outcrops to the interior ocean. Using this model, we are able to quantify water parcel pathways, transit time, and heat transport, providing a unique perspective to evaluate the impact of localized ocean mixing on the large-scale circulation. Second, these simulations provide additional tests and evaluations of the LOM, which is in active development.

The paper is organized as follows. Section 2 presents a brief review of the LOM and the design of the numerical experiments. In section 3, we define and discuss the aTTD method as a tool to diagnose ventilation pathways. In section 4, we present the results from the numerical experiments, including temporally and spatially averaged fields. Finally, in section 5, we offer some concluding remarks and comment on the future development and application of LOM in particular for studying biogeochemical processes.

2. Model description

We briefly describe the basic structure of the model in this section. The details of the LOM are presented in

previous papers (Haertel and Randall 2002; Haertel et al. 2004, hereafter HRJ04; Haertel et al. 2009, hereafter HVJ09), and readers familiar with the model architecture may proceed to section 2b.

a. Model equations

The fluid in the domain is divided into parcels, following the method described in HRJ04. Each parcel is assumed to have a constant horizontal mass distribution given by

$$m_i(x', y') = \frac{M_i}{r_x r_y}[1 + (2|x'| - 3)(x')^2] \times [1 + (2|y'| - 3)(y')^2], \quad (1)$$

where r_x and r_y are the sack radii, $x' = (x - x_i)/r_x$, and $y' = (y - y_i)/r_y$. This function is defined to be nonzero only if $|x'|$ and $|y'|$ are both less than one. The vertical thickness of a parcel can be determined by $H_i(x', y') = m_i(x'r_x, y'r_y)/\rho$.

The predictive equations for each parcel, invoking the hydrostatic approximation, are

$$\frac{D\mathbf{u}_i}{Dt} + 2\Omega \times \mathbf{u}_i = \frac{\mathbf{F}_{p_i}}{M_i} + \mathbf{D}_{v_i}, \quad (2)$$

$$\frac{D\mathbf{x}_i}{Dt} = \mathbf{u}_i, \quad (3)$$

and

$$\frac{DC_i}{Dt} = \mathbf{D}_{C_i}. \quad (4)$$

Equation (2) predicts the momentum for parcel i, Eq. (3) updates the position, and Eq. (4) describes the evolution of a general tracer. In Eq. (2), the pressure gradient ($\mathbf{F}_{p_i}$) can be written (using hydrostatics and water parcel geometry) as

$$\mathbf{F}_{p_i} = \int_A g\nabla H_i \left[\sum_{j=i+1}^{k} (\rho_j - \rho_i) H_j + \gamma\rho_i \left(b + \sum_{j=1}^{k} H_j \right) \right] dA', \quad (5)$$

where the integral over A refers to the horizontal projection of parcel i, b is the height of the bottom topography, k is the total number of water parcels, and A' is a horizontal area increment. We use γ to represent the factor of gravity wave retardation, which is implemented to lengthen the size of the time step and to increase the computational efficiency for the spinup of the model.[1]

Finally, $\mathbf{D}_i$ represents the influence of subgrid-scale diffusion, which is parameterized following HRJ04 and HVJ09. Explicit Eulerian mixing can be applied for each column if desired. This model architecture allows explicit control on viscous friction ($\mathbf{D}_v$) and tracer diffusion ($\mathbf{D}_C$). In practice, $\mathbf{D}_i$ could represent any mixing scheme, from simple constant coefficient mixing to a nonlocal mixing scheme (e.g., *K*-profile parameterization, KPP; Large et al. 1994). In keeping with the idealized nature of this study, we have neglected eddy mixing parameterizations and more complex vertical mixing schemes.

When a water column is statically unstable, the parcels are simply exchanged vertically without transfer of properties between parcels. This treatment of convective instability is a unique feature of the model.

b. Model initialization

This model has been tested in a number of situations, from upwelling in a large lake (HRJ04) to barotropic and baroclinic ocean gyres (HVJ09). The control run is similar to the baroclinic ocean gyre of HVJ09, where the simulated ocean stratification, horizontal currents, and meridional overturning circulation are compared to sister simulations using the Massachusetts Institute of Technology general circulation model (MITgcm). However, in this run, the parcel dimensions are fixed in time, the radius is set to 3°, and the maximum thickness is 24 m.

The model is forced with the zonal wind stress profile shown in Fig. 1a. Temperatures of parcels that reside in the top 50 m of the ocean are restored to the profile in Fig. 1b with a restoring time scale of 30 days^{-1}. In our model we assume a linear equation of state, given by

$$\rho_i = \rho_o(1 - \alpha T_i), \quad (6)$$

where ρ_o is equal to 1000 kg m^{-3} and α is 0.0002°C^{-1}.

Finally, all of our simulations are conducted in a domain that stretches from 20°S to 70°N, 60°W to 0°, and 3000 m in depth.

We will perform and compare three simulations: a constant mixing (CM) run, a focused mixing (FM) run, and a run with a vertical diffusivity based on idealized hurricane-forced mixing. In all simulations, we prescribe the horizontal viscosity to 10^5 m^2 s^{-1}, the vertical

[1] Details of the drawbacks of gravity wave retardation (GWR) and the consequences of its use in the LOM can be found in Haertel et al. (2009) and Jensen (1996, 2001, 2003).

viscosity to 10^{-3} m^2 s^{-1}, and the horizontal diffusivity is set to zero.

In the baseline simulation (CM) vertical diffusivity is set to 5×10^{-5} m^2 s^{-1} everywhere. In the second simulation (FM), the domain-averaged vertical diffusivity is set equal to the baseline simulation, but the entire vertical diffusion occurs within a box extending from the equator to 20°N, 60° to 40°W. The regionally elevated diffusivity, which is set to 5.5×10^{-4} m^2 s^{-1}, is applied through the depth of the modeled ocean for simplicity.[2] Then, we conduct a third simulation, hurricane mixing (HM), where the diffusivity is calculated using Eq. (8) of Korty et al. (2008). In Korty et al., the mixing strength is based on the maximum potential intensity (Emanuel 1988), and in this simulation it is applied to the top 200 m below which diapycnal diffusion is completely suppressed.

To calculate the potential intensity, we have used the SST from the CM run, averaged over the final 10 years. For all other variables, we have utilized monthly averaged 40-yr European Centre for Medium-Range Weather Forecasts (ECMWF) Re-Analysis data. The resulting vertical diffusivity field is given in Fig. 1c. As noted in Korty et al., there is sensitivity to the normalization constants in their Eq. (8). However, since this is an idealized study, we simply choose the normalization constants to keep the maximum diffusivity within a reasonable range (2.5×10^{-4} m^2 s^{-1}).

3. Advective TTDs

We utilize the ability of the LOM to explicitly track water parcels and to characterize water mass ages and transport pathways, including the effects of multiple paths between the surface mixed layer and the interior ocean. Motivated by the TTD of Holzer and Hall (2000), we construct the advective transit time distribution based on the simulated water parcel trajectories. The aTTD is defined as the discrete set of transit times from the surface mixed layer to a control volume in the interior ocean and is determined by tracing the simulated pathways in reverse. During the model simulations, the positions of all water parcels are recorded at a fixed time interval. Once the simulation is completed, we identify a set of parcels within an arbitrarily defined control volume. This volume is bounded by a specified latitude–longitude and density (or depth) range (taken at the end of the simulation).

[2] While there are observations to confirm the presence of elevated mixing in the western tropical Atlantic (Schmitt et al. 2005), there is no evidence for this elevated mixing extending through the entire column.

In our analysis, we typically define a control volume large enough so as to contain a sufficiently large sample size [$O(100)$]. For example, a control volume of 10° (latitude) × 20° (longitude) × 3° (Celsius) (or a few hundred meters) may contain a few hundred parcels. Once all of the parcels are identified in the control volume, we trace their trajectories backward in time until those parcels come in contact with the surface layer.

Our aTTD analyses are discrete (e.g., Fig. 12a), similar to that in Harper (2000) where a defined number of particles are advected in an Eulerian model. In fact, one test case (a ventilated thermocline region) produces a similar histogram to Fig. 5d in Harper (2000).

The transit time analyses presented in this paper are ''advective'' TTDs and there are some notable differences from the standard TTD in the literature. The aTTD accounts for the water mass transport by the resolved circulation reflecting advective and convective transport only. In other words, aTTD does not include the direct effects of subgrid-scale turbulent parameterization, which could play a nonnegligible role in a region such as the equatorial thermocline. Thus, we must use caution to directly compare aTTD and TTD. In the tropical thermocline where vertical stratification might be controlled by the vertical advective–diffusive balance, subgrid-scale diffusion may be moving heat (and other tracers) downward from the surface. At the same time, parcels are upwelling from below. When the trajectories are constructed, we will find the parcels that enter the control volume from upstream regions only. On the other hand, in a standard TTD calculation, where a dye tracer is injected into the surface layer, some tracer will diffuse into the equatorial thermocline from above, which may give an apparent bias to the aTTD relative to the standard TTD.

Each element of the discrete aTTD is associated with the three-dimensional pathway that offers a new perspective on tracer ages and transport pathways focusing on the effects of resolved advective transport, explicitly connecting the surface mixed layer to the interior ocean. However, hundreds of trajectories would be very complex and difficult to interpret objectively. Therefore, we construct the Lagrangian streamfunction based on the collective volume transport of the sack ensemble that is found within the control volume (as in Döös 1995). Lagrangian streamfunctions were first introduced by Blanke et al. (1999) and have been used in a number of studies (e.g., Döös and Engqvist 2007; Döös et al. 2008). This can allow us to quantify and display the collective pathways of all the parcels in a given region.

To calculate the Lagrangian streamfunctions, trajectories for a given control volume are interpolated to a grid,

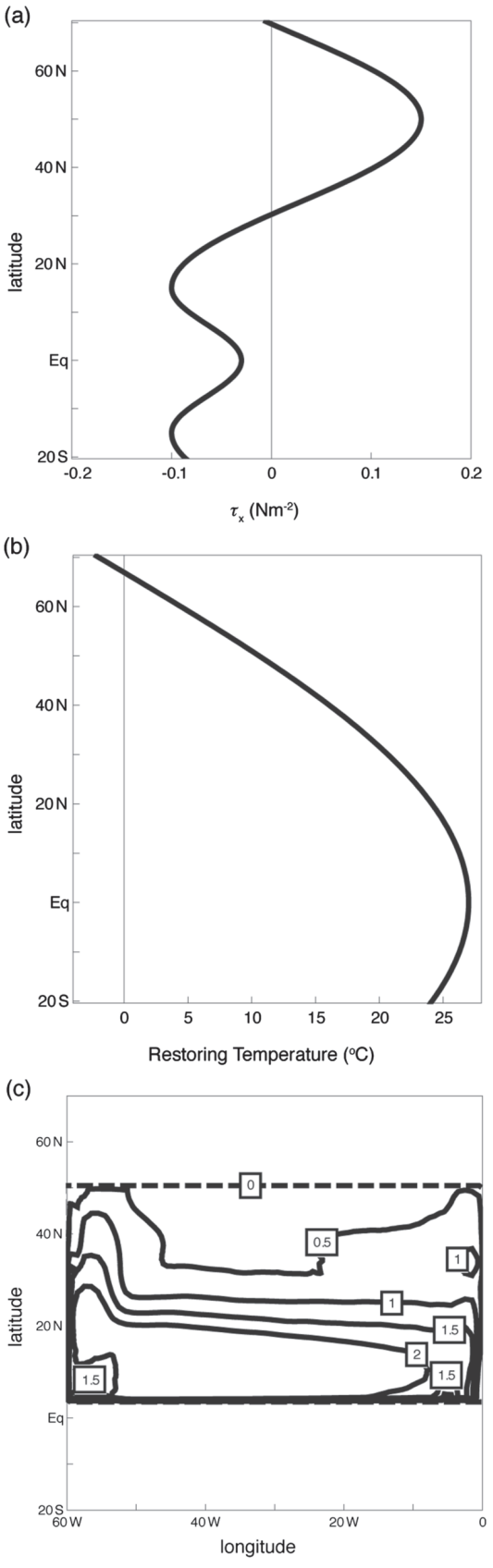

and the remaining computation proceeds as described in previous papers (e.g., Döös et al. 2008, appendix A).

4. Results

Three simulations are carried out to characterize and describe the response of large-scale ocean circulation to highly localized diapycnal mixing including a constant mixing run, a focused mixing run, and the hurricane-induced mixing run. We show that the LOM is able to reproduce essential features of large-scale ocean circulation and exploit the advantages of the Lagrangian model to present insightful and unique diagnostics of the oceanic transport of heat and tracers.

a. Meridional overturning circulation

In each experiment, the model is spun up for 1000 years. The circulation reaches a quasi-steady state after 200 years of integration and does not change significantly afterward. To determine time-averaged results, we average over the final 15 yr of the run (at 100-day intervals). The time-averaged (years 985–1000) MOCs for all three experiments are presented in Fig. 2. The contour interval is 2 Sv (Sv $\equiv 10^6$ m^3 s^{-1}).

In the CM run, the maximum deep overturning is 12.2 Sv, which is broadly similar to previous Eulerian model results (e.g., Marotzke 1997; Ito and Follows 2003). The maximum deep overturnings for the FM and HM runs are 11.6 and 4.4 Sv, respectively. The similarities between the FM and CM runs are the result of two competing effects. First, the FM run may have greater domain-integrated diapycnal buoyancy fluxes. The elevated diapycnal diffusivity of the FM run is calculated such that the domain-integrated diffusivity would be the same between the CM and the FM runs. As argued in Scott and Marotzke (2002), the domain-integrated diffusivity should exclude high-latitude regions where the static stability is very low (where constant mixing would have little effect). In the extremely localized mixing case of Scott and Marotzke, the diffusivity in the mixing column is set equal to the area-integrated diffusivity south of 36°N. Inclusion of the high latitudes

←

FIG. 1. Plots of the surface boundary conditions: (a) the zonal component of the surface wind stress (the meridional component is set to zero everywhere) and (b) the restoring temperature. Both profiles in (a) and (b) are assumed to be independent of zonal position. (c) The map of vertical diffusivity (units of 10^{-4} m^2 s^{-1}) for the HM run (equal to zero south of 5°N and north of 50°N). These diffusivities are applied to the top 200 m and are set to zero at all other depths.

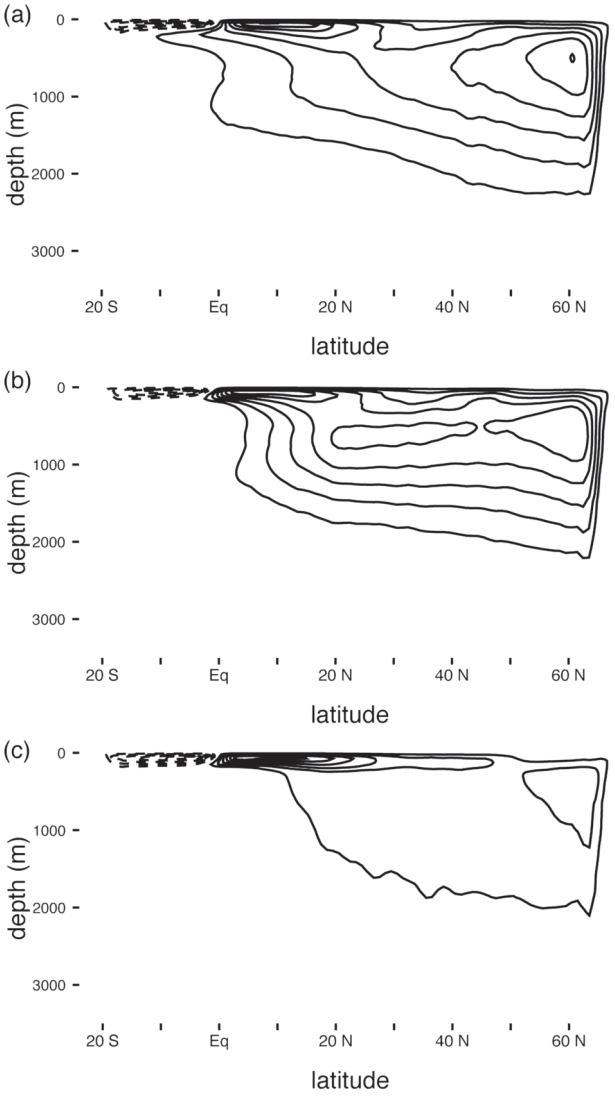

FIG. 2. Meridional overturning streamfunctions in depth coordinates for the (a) CM, (b) FM, and (c) HM runs. The contour interval in all plots is 2 Sv. These results have been averaged over the final 15 yr of the runs.

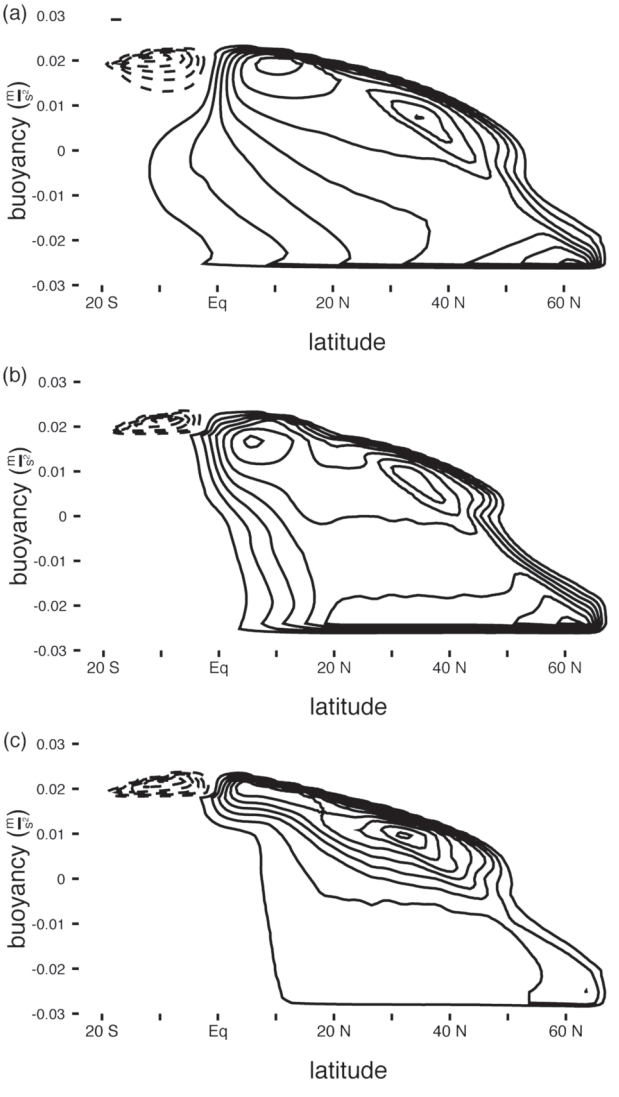

FIG. 3. As in Fig. 2, but presented in a buoyancy coordinate.

increases our diffusivity by about 25% compared to Scott and Marotzke (2002).

Second, the surface buoyancy gradient in the FM run is slightly weaker than that of the CM run. When diapycnal diffusion is locally enhanced, the upwelling of relatively cold, deep waters tends to lower the surface temperature. When the mixing is forced into a single column, as in the case of Scott and Marotzke, the cooling effects of the diffusively driven upwelling on the SST overwhelms the surface restoring, resulting in a weaker MOC by reducing the lateral buoyancy gradient. In the FM run, the region of enhanced mixing covers a relatively large area, and its impact on the SST is only about 2°. Overall, the FM run has slightly stronger downward diffusion of heat and hence a stronger MOC.

In the HM run, the deep overturning is much weaker than in the other two runs because vertical diffusivity is nonzero only in the upper 200 m. In this case, the abyss is very weakly stratified and filled with the coldest surface water. This will give a much weaker and shallower overturning.

All Lagrangian streamfunctions are presented in a density coordinate. To facilitate comparison, we calculate the overturning streamfunction for the three runs on the same density coordinate (Fig. 3). Note that most of the overturning in Fig. 3c occurs within a few hundred meters of the surface because of the strong near-surface stratification and very weakly stratified deep ocean. If the MOC were plotted on the z coordinate, the deep

overturning circulation would appear to be almost stagnant (Fig. 2c). This plays an important role in our discussion of Lagrangian streamfunctions.

b. Averaged temperature, velocity, and transport

The meridional sections of temperature from the three runs show the differences in thermal structure and stratification due to the differences in the diapycnal diffusion and meridional overturning circulation. The relatively strong downward heat flux of the FM run makes the abyss slightly warmer in comparison to the CM and HM runs. On the eastern boundary (Fig. 4), the abyssal temperature is warmest in the FM run (Fig. 4b), even though the eastern boundary is outside the area of enhanced mixing.

The differences in deep ocean temperature, especially in the polar regions (north of 45°N and deeper than 200 m) could be attributed to stronger advective downwelling in the FM run, which is driven by the enhanced vertical diffusivity at low latitudes.

The horizontal velocity fields for the upper ocean are shown for the three runs in Figs. 5–7 . Panel a in all three of these figures is the surface (0–50 m) and panel b is the thermocline (150–350 m). In Figs. 5a, 6a, and 7a, the advective downwelling is strongest in the northeast corner of the model domain. The FM run exhibits the strongest polar sinking and the HM run is the weakest, consistent with the deep penetration of relatively warm temperatures in the FM run compared to the other two runs.

As expected, the shallowest thermocline occurs in the HM run. The lack of vertical diffusion below 200 m causes the abyss to fill up with the coldest surface water, confining the overturning to the top 200 m. Away from the subpolar gyre, the velocity fields from the three runs appear to be similar both at the surface and near the thermocline. At low latitudes, the model captures the broad structure of the equatorial currents in all the runs.

In the abyssal layers (1900–2100 m), the velocity fields share basic common features, such as deep western boundary currents, but they do not appear to be as similar as the upper oceans (see Fig. 8).

The abyssal velocity field from the CM run (Fig. 8a) is characterized by a southward flow near the western boundary and a northward return flow in the interior ocean, similar to the classical model of the abyssal circulation (Stommel and Arons 1960). In the FM run, the field is slightly more complex. In addition to the deep western boundary current, there is a strong northward flow in the region where intense vertical mixing is imposed and a low-level convergence is observed [as in the localized mixing case of Scott and Marotzke (2002)]. The flow field in the HM run (Fig. 8c) is broadly similar to the CM run, including the southward deep western boundary current and the signature of a wind-driven, subpolar gyre at high latitudes.

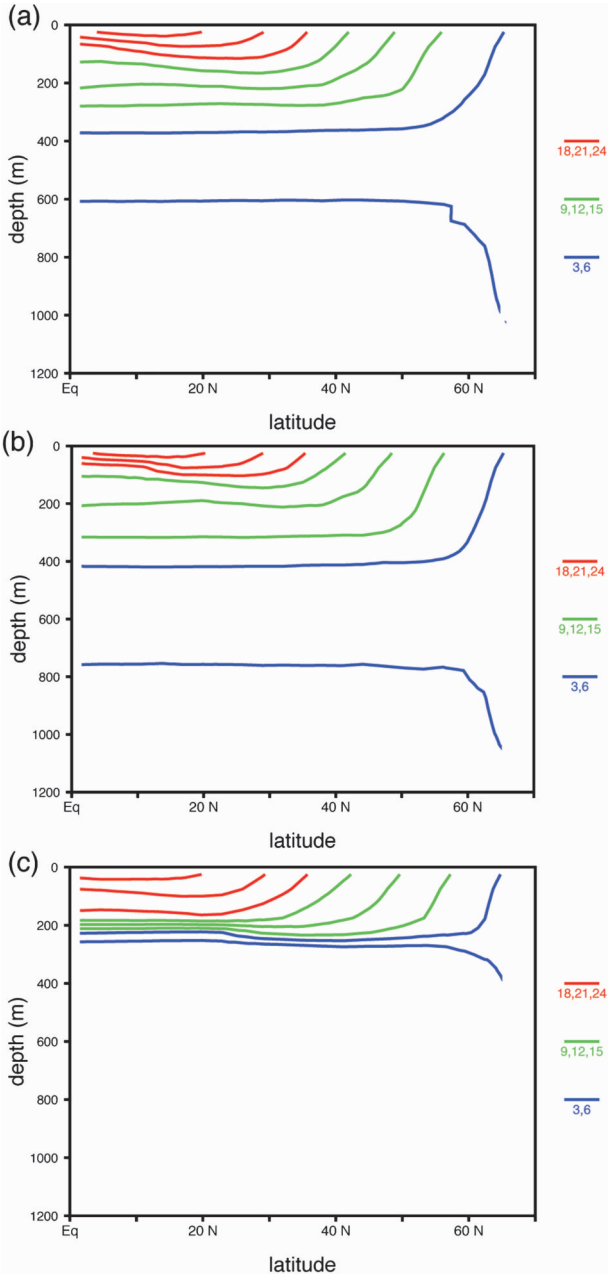

FIG. 4. Latitude vs depth profile of temperature at 5°W for the (a) CM, (b) FM, and (c) HM runs.

The pattern and magnitude of the meridional heat transport are similar between the CM and the FM runs, consistent with similar structures in the respective MOCs. The northward heat transport in the FM run is slightly stronger relative to the CM run, which could be due to the slightly stronger area-weighted vertical diffusivity. The location of a focused mixing region in the

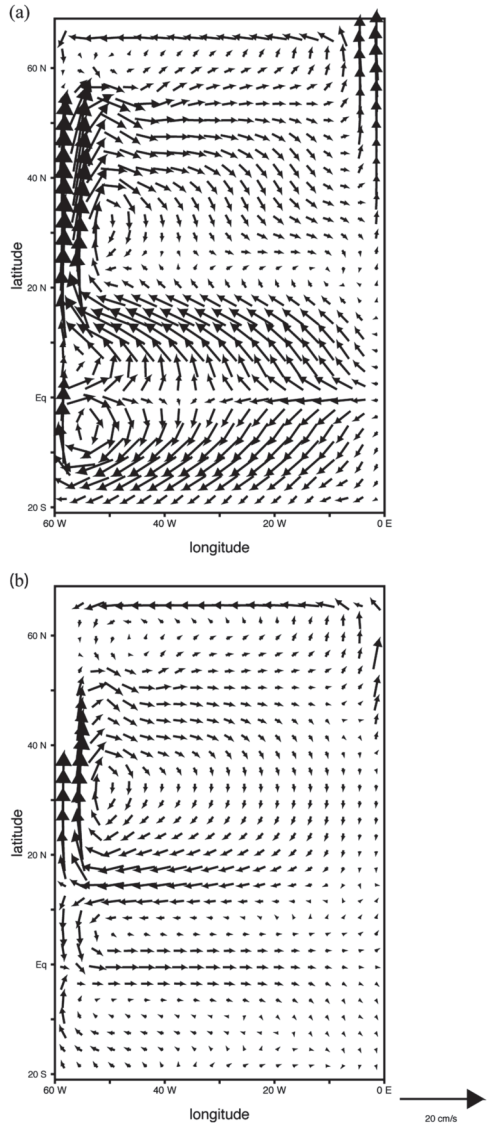

FIG. 5. Lateral velocities for the CM run averaged over the (a) top 50 m and (b) 150–350-m depth.

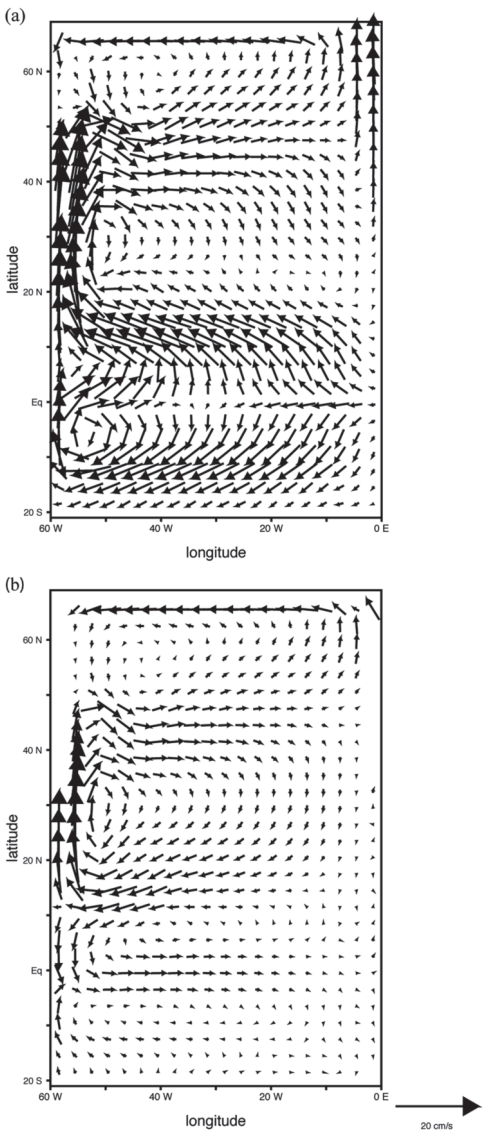

FIG. 6. As in Fig. 5, but for the FM run.

tropics strengthens upwelling since we have placed elevated vertical diffusivity where advective diffusive balance dominates, consistent with Colin de Verdière (1988). The heat transport profile for the HM run exhibits a similar shape to the other runs, but the magnitude is weaker since the abyssal MOC transports little heat.

Figure 9 shows the distribution of meridional volume transport in the western boundary current region (15°–50°N, 60°–54°W; black for the CM run, dashed for the FM run, and gray for the HM run) subdivided into density (equivalently, temperature) classes (constructed following Samelson 1998, Fig. 16).

As expected, the southward transport of the coldest waters is greatly reduced in the HM run when compared to the other runs due to the lack of diapycnal diffusion in the deep ocean. Figure 9 also shows that the FM run has stronger southward transport of colder water. In general, the transport in the FM run is stronger in nearly all temperature classes less than the surface temperature (~24°C).

c. *Trajectories and aTTDs*

Here we characterize the spatial and temporal structures of the simulated circulation fields using the concepts of aTTD and the Lagrangian streamfunction. In particular, we determine the transit time of water masses from the surface mixed layer to a chosen region in the interior ocean along with the associated three-dimensional

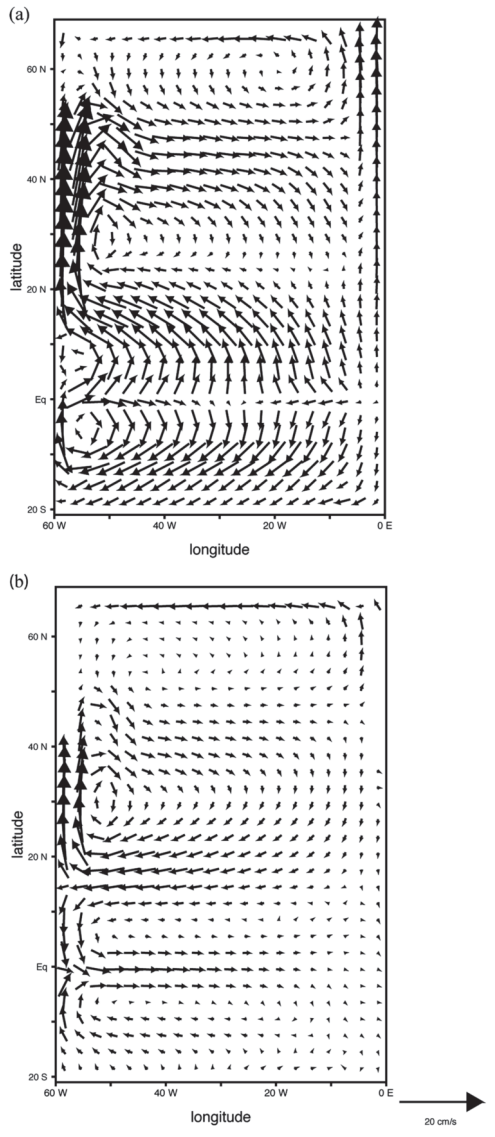

FIG. 7. As in Fig. 6, but for the HM run.

pathways. For this analysis we choose three different regions as control volumes: 1) tropical thermocline, 2) ventilated thermocline, and 3) abyssal ocean.

1) CONTROL VOLUME 1: EQUATORIAL THERMOCLINE

The first control volume is in the equatorial thermocline (2°–12°N, 40°–20°W, 150–350-m depth). The discrete aTTDs from the three runs (CM, FM, and HM) are presented in the form of histograms in Figs. 10a–c, respectively. The first and second moments of the aTTDs can be found in Table 1. The aTTD for the CM run has two distinct peaks: one on the decadal time scale and the other at about 100 yr (mean age 116.43 yr).

The bimodal structure is not evident in the FM run, which shows a single peak at about 50 yr (mean of 73.81 yr), where the youngest mean age of all the runs is consistent with the strong diapycnal diffusion and vigorous overturning circulation. The aTTD for the HM run is much older (mean of 372.6 yr), reflecting the significantly weaker diapycnal diffusion and overturning circulation below the depth of 200 m.

To visualize the pathways of water masses associated with the aTTDs, the Lagrangian streamfunctions (from here onward, anytime streamfunction is used, Lagrangian is implied) are presented in Fig. 11, where the barotropic streamfunctions are on the left and the meridional overturning counterparts are on the right. In all of the barotropic streamfunctions, the dashed gray box demarcates the ending point for our parcels. In the baroclinic plots, the solid gray box represents the buoyancy interval for the given box.

All of our control volumes were defined in height. To plot the gray boxes (see Figs. 11, 13, and 15), we took the time-averaged (~10 yr) and zonally averaged buoyancy profiles and inverted them to find the corresponding depth values. In all of the following plots of the streamfunctions, the contour interval is set to 0.25 Sv.[3]

There are two preferred pathways for the control volume in the tropical thermocline. One nearly conserves buoyancy, originating from the isopycnal outcrop location in the middle latitudes, and the other is a deep pathway. The two distinct pathways in the CM run provide the key to understanding the bimodal structure of the associated aTTD.

The stronger deep overturning in the FM run (3.5 Sv, Fig. 11d) relative to the CM run (1.5 Sv, Fig. 11b) is due to the proximity of the focused mixing box to this particular control volume and is responsible for the relatively young mean age in the FM run. Further, the pattern of the upwelling of deep water is fundamentally different between the CM and the FM run. The upwelling is intense and concentrated in the focused mixing region in the FM run. In contrast, the deep waters rise relatively slowly over a broad area in the CM run, which can be seen in the curved stream lines in Fig. 11b compared to the nearly vertical lines in Fig. 11d.

In the HM run, diapycnal diffusion is only nonzero above 200 m. Below this level, the waters are nearly isothermal with an abyssal temperature. Some of the waters in this control volume can quickly rise to the

[3] It is difficult to determine the actual horizontal pathway from the barotropic streamfunctions, as these include the surface gyre contribution and the deep ocean circulation. To better interpret water mass pathways, we also rely on the vector velocity fields (Figs. 5–8).

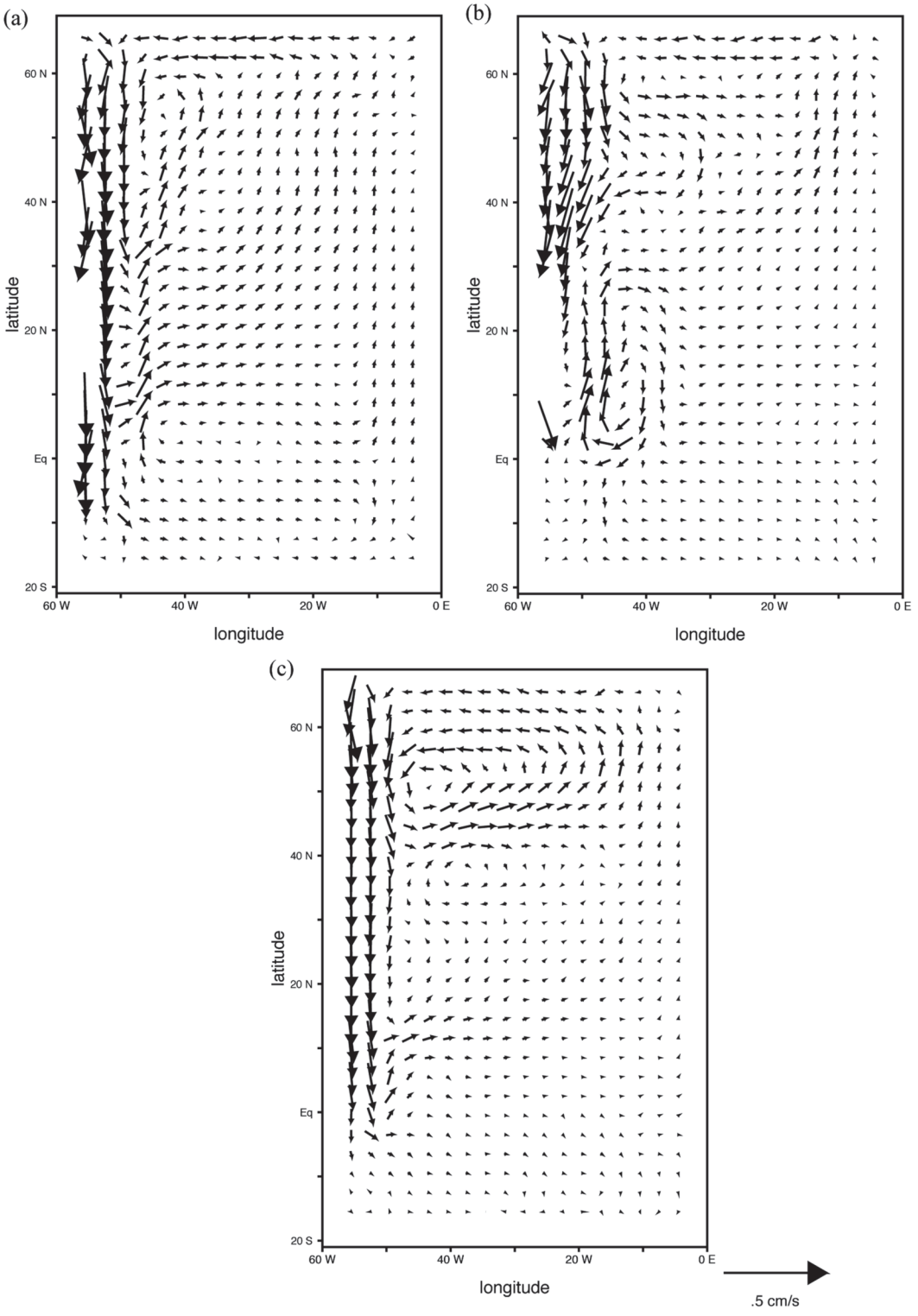

FIG. 8. Deep ocean velocities (1900–2100 m) for the (a) CM, (b) FM, and (c) HM runs. Velocities greater than 0.5 cm s^{-1} have been omitted to emphasize the interior circulation.

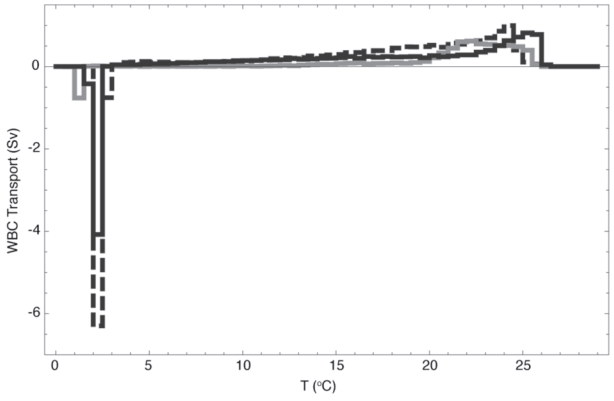

FIG. 9. Western boundary current transport by temperature class (calculated following Samelson 1998, Fig. 16). The CM run is black, FM is dashed, and HM is gray. The results have been averaged over the final 10 yr of the run.

surface, as shown by the tightly packed contours near the top of the gray box in Fig. 11f. These water parcels are influenced by the wind-driven divergence of the horizontal currents at the surface on the eastern boundary near the equator. The upwelling deep waters are transported from the abyss to the eastern tropical region by the equatorial undercurrent (see Fig. 7b). Then, the waters rise toward the surface and rapidly increase their temperatures once they enter into the depth range where the diapycnal diffusivity is nonzero. The parcels that are warmest and farthest north in the control volume follow a shallow trajectory in all runs. Figures 11b, 11d, and 11e show that the trajectories depart the surface near 40°N, or the subtropical–subpolar boundary, where these parcels are subducted into the interior, flowing southward in the subtropical gyre to reach the control volume.

2) CONTROL VOLUME 2: VENTILATED THERMOCLINE

Here the control volume is defined in the ventilated thermocline (25–35°N, 40°–20°W, and 200–400 m). The aTTDs for the CM, FM, and HM runs are shown in Figs. 12a–c, respectively. The three histograms are broadly similar, as the structure of the ventilated thermocline does not depend on the details of the diapycnal diffusion. In all three runs, a strong peak is present on the decadal time scale with a well-defined tail (out to approximately 200 yr).

The barotropic and baroclinic streamfunctions for the three runs (Fig. 13) show that the shortest trajectories to the surface are nearly adiabatic, indicative of the wind-driven ventilated thermocline. There is some tilt to the streamlines in Fig. 13b (CM run), indicating some diabatic movement, consistent with the CM run having nonzero

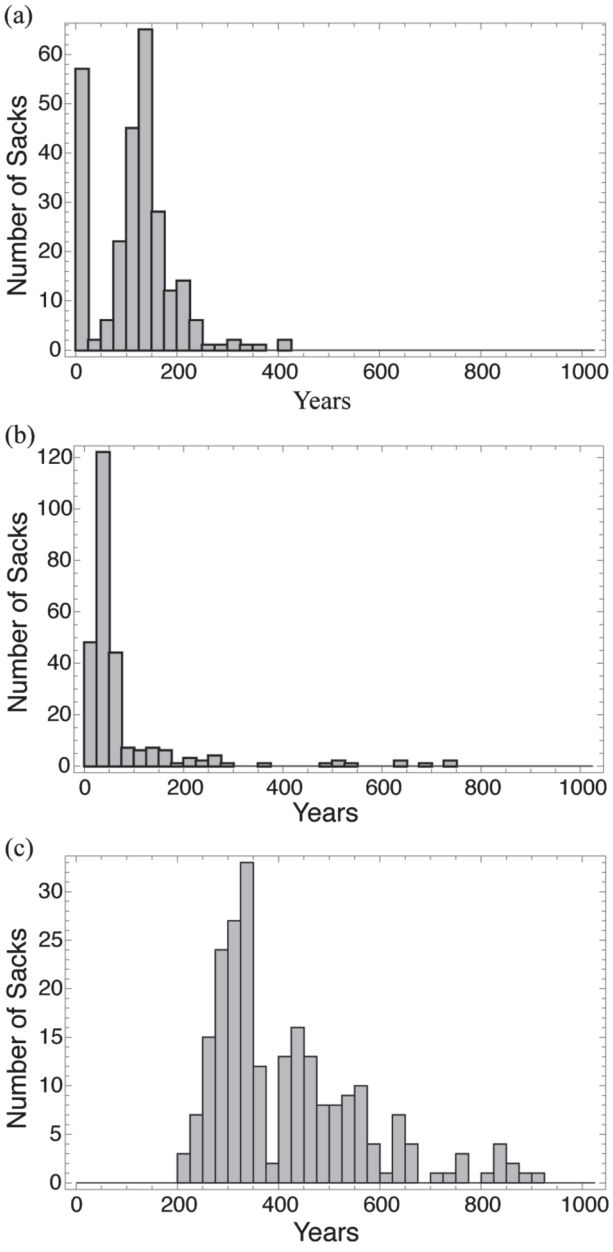

FIG. 10. The aTTD histogram for the control volume spanning 2°–12°N, 40°–20°W, and 100–300 m in depth for the (a) CM, (b) FM, and (c) HM runs.

diffusivity north of 50°N (the HM and FM runs have zero diapycnal diffusivity in the high latitudes). In the FM and HM runs, the parcels are subducted from the surface and move toward the control volume nearly adiabatically, following the streamlines of the subtropical gyre.

Figure 13d shows a transport of about 4 Sv through the control volume, by far the strongest of the runs, consistent with the youngest mean age for the FM run. The CM run has an average of about 2 Sv in the control volume, while

TABLE 1. First and second moments of the aTTD histograms. Results are presented for the three runs and all control volumes.

Run	Mean	Std dev
Equatorial thermocline		
CM	116.43	74.87
FM	73.81	116.33
HM	372.60	309.50
Ventilated thermocline		
CM	41.18	68.34
FM	21.14	43.68
HM	160.51	314.46
Abyssal ocean		
CM	277.36	193.90
FM	214.06	337.55
HM	419.36	150.43

the HM run has an average of about 1 Sv. In the HM run, there is evidence of multiple pathways. Examining Fig. 13f, parcels in the upper portion of the control volume follow the trajectory described above. However, the parcels near the bottom of the control volume follow a diabatic pathway. Because much of the buoyancy variation occurs in the top 200 m, the diabatic pathway is also confined within the shallow depths where the parcels move southward from the subpolar gyre, get entrained into the subtropical gyre, and finally enter the control volume. This particular pathway is of secondary importance to the ventilation of the control volume since the transport is only 0.75 Sv.

3) CONTROL VOLUME 3: ABYSSAL OCEAN

Here the control volume is located at the base of the modeled overturning circulation to evaluate the deep ventilation pathways (25°–35°N and 40°–20°W, 200 m thick, centered at 2000-m depth). Figure 14 displays the discrete aTTDs for this control volume. The CM and the FM runs are similar to one another (Figs. 14a and 14b). However, the HM run aTTD is significantly different (Fig. 14c). The aTTDs of the CM and FM runs peak at about 150 yr with mean ages of 277.36 and 214.06 yr, respectively. In contrast, the aTTD of the HM run peaks near 325 yr with the mean age of 419.36 yr.

In these calculations, a fraction of the reverse trajectories are not in contact with the surface even after the 1000 years of model integration. The length of the run was not long enough to completely replace all of the deep waters with newly formed waters. Superimposing the location of this control volume on top of Fig. 8b can qualitatively illustrate the lateral trajectories leading to the control volume from the region of the deep-water formation in the northwest corner of the domain. Parcels must flow southward in the deep western boundary current toward the equator where they spread to the interior ocean and turn to the north. The location of this particular control volume is farther downstream of this deep circulation and it could take a long time to ventilate this control volume. Similar numbers of reverse trajectories reach the surface in the CM and HM runs. Therefore, the aTTDs for this particular control volume have a long tail, which is truncated at 1000 yr.

The streamfunctions for this control volume are given in Fig. 15. Immediately, we notice the weakness of the streamfunctions for the CM (and FM) run compared to the previous control volumes. The deep circulation due to the parcels in the control volume is about 0.5 Sv, a very small percentage of the transport due to all of the parcels (cf. Fig. 3). The pathway from the surface to this control volume is primarily along the constant buoyancy surface, and its horizontal path essentially follows the circulation pattern from the classical solution of Stommel and Arons (1960).

Figure 15a, the horizontal circulation pattern, shows significant differences from the upper-ocean wind-driven gyres (compared to Fig. 13a especially). There is a barotropic transport cancellation between the deep western boundary current and the surface western boundary current. Further, the northward flow in the abyssal interior and the tropical gyre (northward as well) lead to the deformation of the subtropical gyre with a maximum transport of 0.75 Sv.

The streamfunctions, in Figs. 15c and 15d, are broadly similar to those in the CM run. In the FM run, the trajectories follow a path to the control volume that is nearly adiabatic. Even though the barotropic streamfunctions are similar for the FM and CM runs, the individual pathways at depth are quite different. Recalling Fig. 8b, there are trajectories in the FM run that circulate in a small loop near the mixing box, which is different from a circulation inferred from Stommel–Arons theory because the majority of the vortex stretching only occurs in the focused mixing region (Sverdrup flow cannot support meridional motion outside of the focused mixing region).

The most remarkable result is for the HM run (Figs. 15e and 15f), where the MOC is more than four times stronger near the surface relative to the CM and FM runs. The deep ocean overturning remains roughly the same (about 0.5 Sv). The barotropic streamfunction is only slightly weaker than that for the other control volumes of the HM run (Figs. 11e and 13e). The apparent strength of the MOC from the HM run is somewhat counterintuitive as there is no diapycnal diffusion below 200 m. In fact, the abyssal circulation involving the densest water masses is roughly equal between all of the runs. However, the HM run has a much stronger upper-ocean circulation. The apparent strength of the MOC in the upper ocean could be driven by an intense recirculation

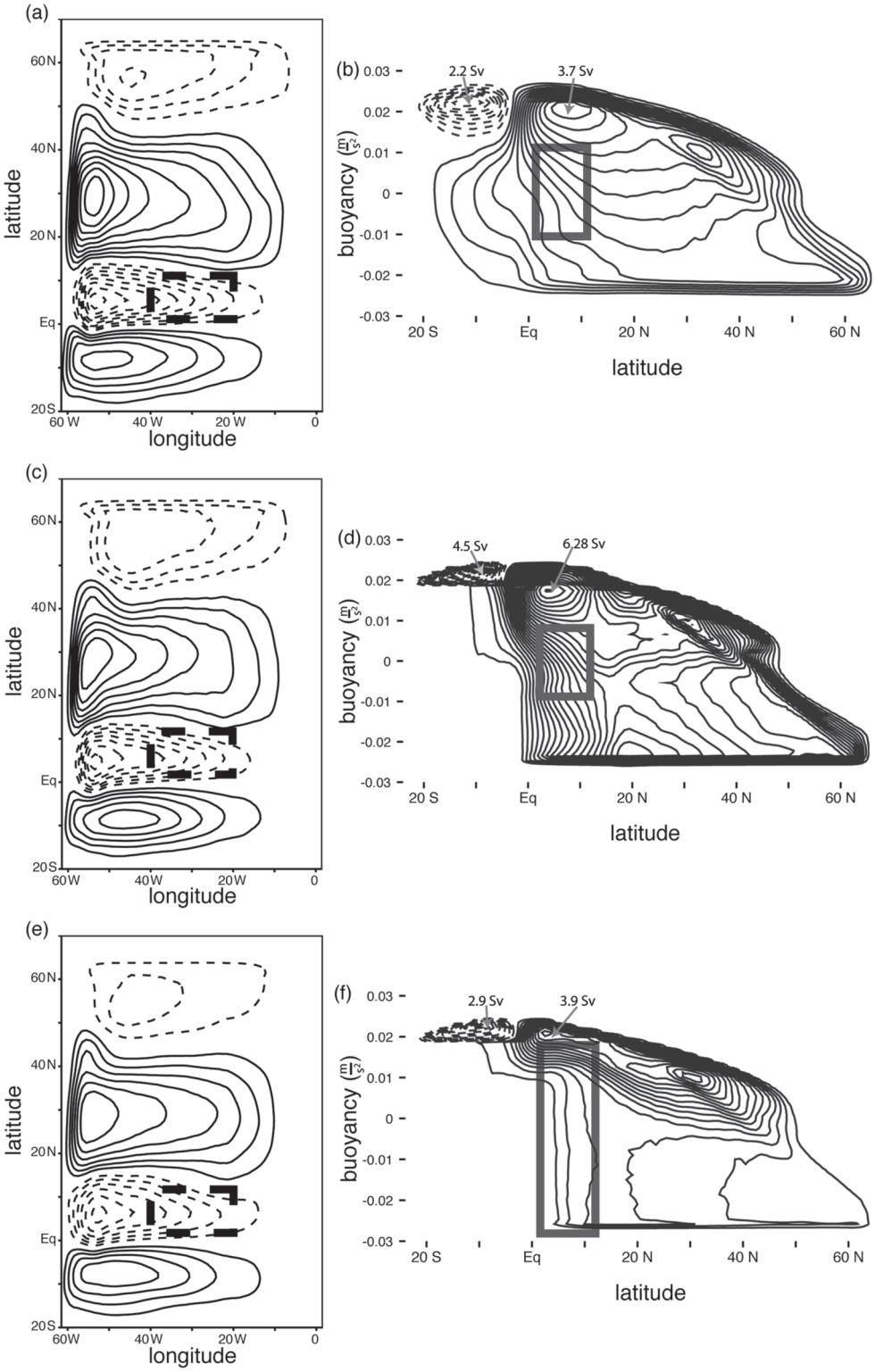

FIG. 11. (a) Barotropic and (b) baroclinic Lagrangian streamfunctions for the CM run. (c),(d) As in (a),(b) but for the FM run; (e),(f) as in (a),(b) but for the HM run. The plots are generated from trajectories ending in the control volume spanning 2°–12°N, 40°–20°W [dashed black box in (a)] and 100–300 m in depth. The equivalent span in buoyancy (calculated from the zonally integrated buoyancy averaged over the final 10 yr) is demarcated by the gray box in (b). The contour interval is 0.25 Sv.

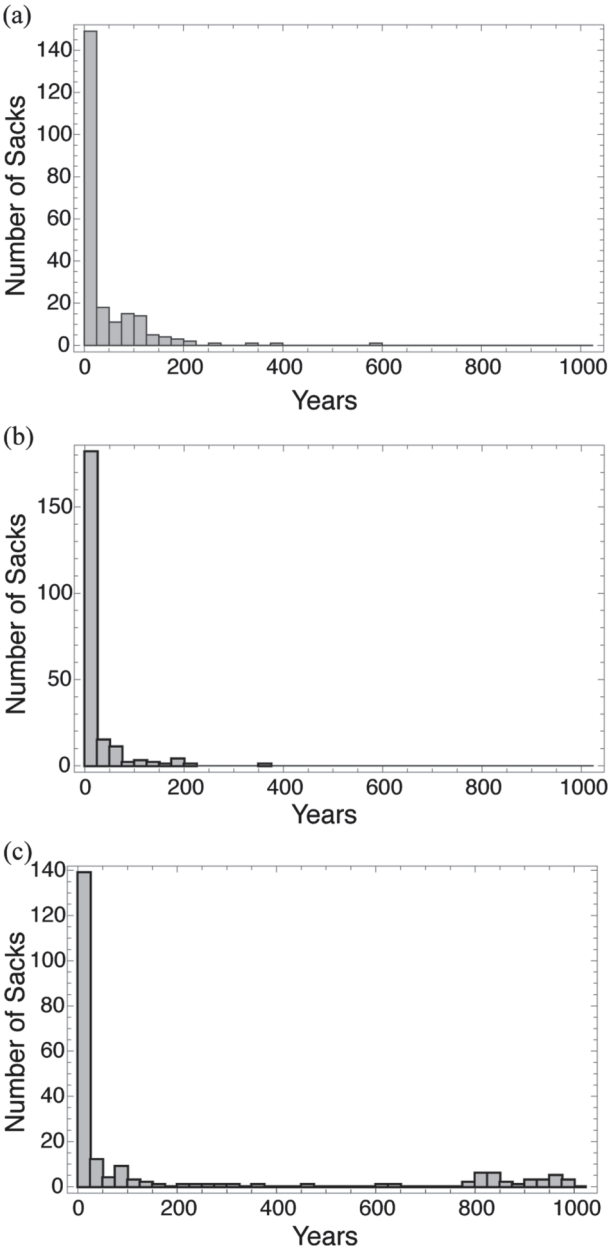

FIG. 12. The aTTD histogram for the control volume spanning 25°–35°N, 40°–20°W and 200–400 m in depth for the (a) CM, (b) FM, and (c) HM runs.

within the top 200 m. When the streamfunctions are constructed, the influence of the individual parcel is not terminated until the trajectory is closed in the three-dimensional space where buoyancy is used as the vertical coordinate. In the HM run, the choice of the vertical coordinate can impact the presentation of the streamfunction, especially for the weakly stratified abyss because a wide range in height is compressed into a narrow buoyancy range. This implies that the circulation in Figs. 15e and 15f may not be closed in height space even though they are closed in buoyancy space.

A portion of the horizontal trajectories at depth may be explained by intense vertical momentum diffusion. In Fig. 8c, we can see a fairly well-defined subpolar gyre similar to the surface circulation. There is a slow southward flow into the control volume from the north and one flowing into the box from the south. The parcels entering from the north are most likely responsible for the younger portion of Fig. 14c, while those entering from the south would be older.

5. Conclusions

In this study, the Lagrangian ocean model (LOM) is used as a tool to examine the Lagrangian pathways of water parcels in a wind- and buoyancy-driven meridional overturning circulation in an idealized ocean basin. The primary goal of this study is to evaluate the response of the meridional overturning circulation to a spatially variable diapycnal mixing from a Lagrangian perspective.

Owing to the Lagrangian formulation of the model, we are truly able to constrain the rate of tracer diffusion, which makes it possible to focus diapycnal diffusion within a limited region. Furthermore, the model is able to explicitly calculate the positions, velocities, and tracer properties of water parcels in the model domain. Taking advantage of these features, we develop a new diagnostic to analyze the water mass ages by tracking the positions of water parcels backward in time. The resulting discrete distribution of transit time is termed an advective transit time distribution (aTTD), which represents the probability distribution of the transit time intervals between the surface mixed layer and the interior ocean, which are associated with three-dimensional pathways of water parcels. This new diagnostic can quantitatively connect the physical circulation following water parcels and the probability distribution of water mass ages in a clear and transparent way, providing insights into the physical mechanisms controlling the impact of intense localized mixing on the meridional overturning circulation.

a. Key results of the sensitivity experiments

We examined the classical problem of a wind- and buoyancy-driven circulation in a single-hemispheric ocean basin. Within this framework, we conducted three simulations, including a control run (uniform diffusivity), a run with localized diapycnal mixing, and a run with the vertical diffusivity profile based on an idealized hurricane-induced mixing (adapted from Korty et al. 2008). Similar experiments have been carried out using Eulerian ocean models and the overall results are

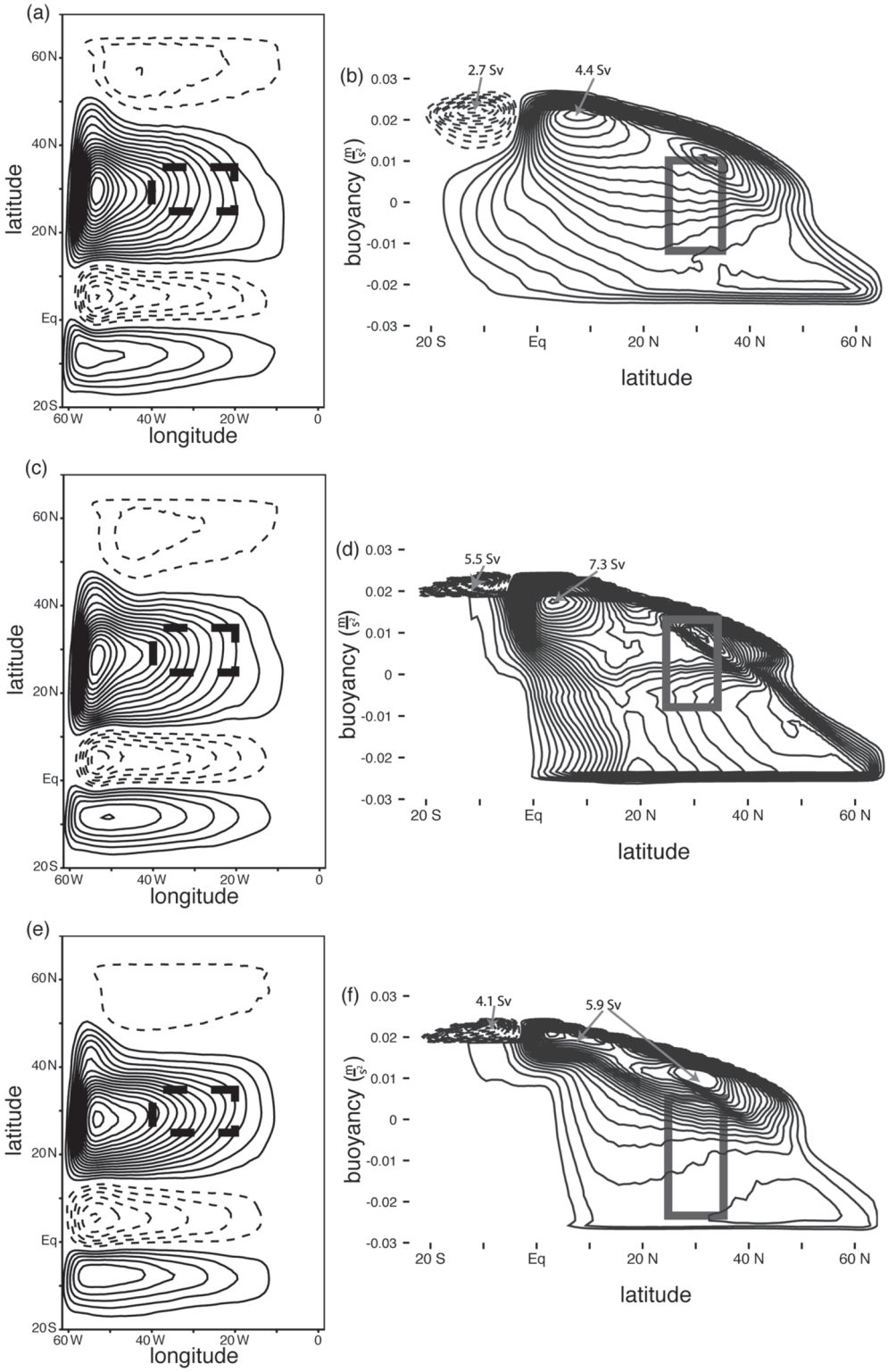

FIG. 13. (a) Barotropic and (b) baroclinic Lagrangian streamfunctions for the CM run. (c),(d) As in (a),(b) but for the FM run; (e),(f) as in (a),(b) but for the HM run. The streamfunctions were calculated from the trajectories ending in the control volume spanning 25°–35°N, 40°–20°W [dashed black box in (a)] and 200–400 m in depth. The equivalent span in buoyancy (calculated from the zonally integrated buoyancy averaged over the final 10 yr) is demarcated by the gray box in (b). The contour interval is 0.25 Sv.

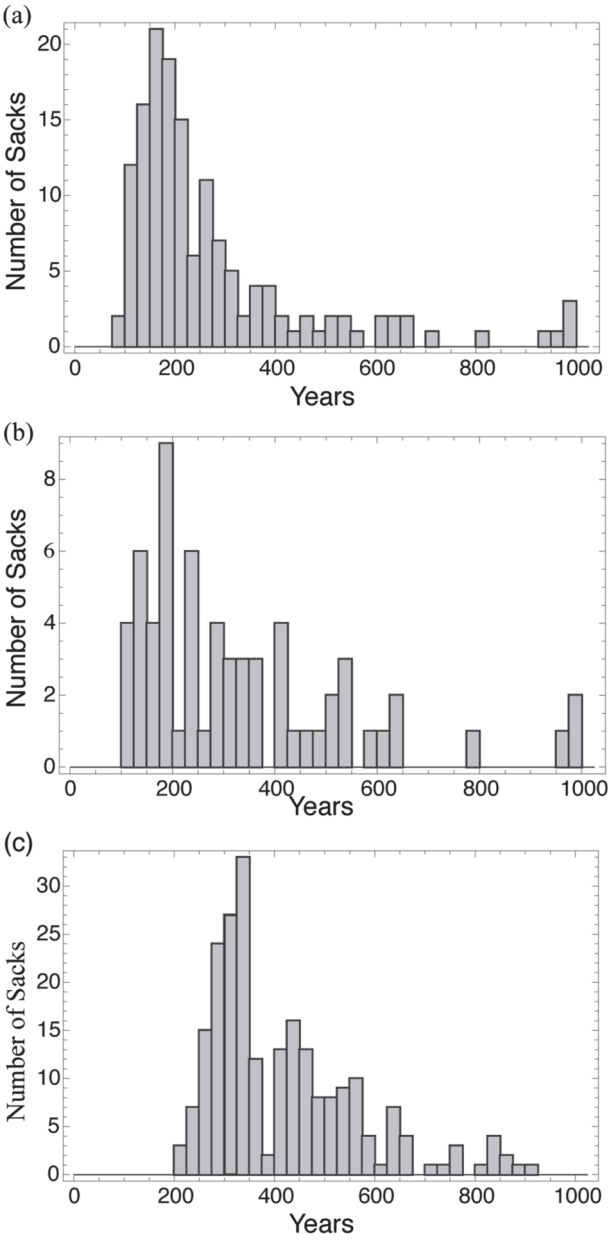

FIG. 14. The aTTD histogram for the control volume spanning 25°–35°N, 40°–20°W and 1900–2100 m in depth for the (a) CM, (b) FM, and (c) HM runs.

qualitatively similar (Huang and Chou 1994; Marotzke 1997; Samelson 1998; Scott and Marotzke 2002).

In our study, the temporally and spatially averaged circulations and the heat transport are broadly similar between the control and the focused mixing experiments, which is most likely the result of two competing effects. First, we constrained the area-integrated diffusivity to be the same between the control and the focused mixing runs, where the area integration included the high latitudes where the water column is weakly stratified. The vertical diffusivity is enhanced in the focused mixing run within a specific region in the low latitudes where the stratification of the water column is stronger than the global average. This increases the net diapycnal diffusion of buoyancy in the focused mixing run. Second, since the enhanced mixing is placed where surface heating occurs, the enhanced diapycnal diffusion brings up cold abyssal water, working against the effects of surface heating. This would result in a weaker overturning (as in Scott and Marotzke 2002). In combination, these two effects result in similar overturning circulations and heat transports between the uniform mixing and the focused mixing run.

In the hurricane-induced mixing run, the temperature profiles and time-averaged MOC show a much less effective transportation of heat. In particular, the simulated thermocline and the overturning circulation are much shallower than in the other two runs due to the lack of the diapycnal diffusion below 200 m. In this case, the deep ocean is filled with the coldest surface water, confining the overturning circulation to shallow depths.

The aTTD is constructed from the three model runs using reverse trajectories. Furthermore, the Lagrangian streamfunction is constructed following Blanke et al. (1999) and Döös et al. (2008) and is associated with each aTTD, which reveals important regional differences in ventilation pathways and water mass ages. First, we identify two major ventilation pathways of tropical thermocline water. Some water parcels travel primarily along isopycnal surfaces from the subpolar–subtropical gyre boundary to the tropical thermocline (adiabatic pathway). Other water parcels sink at the polar oceans and travel through the deep western boundary current equatorward and upwell into the low-latitude thermocline through diapycnal mixing (diabatic pathway).

The water mass age, as defined by the first moment of the aTTD, is sensitive to the pattern and magnitude of the diapycnal diffusion. The mean age is significantly different between the control and the focused mixing run because of the intense, localized upwelling in the focused mixing run. In all of our control volumes, the mean age is longest for the HM run. Table 1 summarizes the mean ages of different water masses. Locally enhanced mixing in the western tropical thermocline leads to younger water mass ages in the tropical thermocline by about 30%. In the ventilated thermocline nearly all trajectories in the three runs follow the ventilation pathway, as predicted by Luyten et al. (1983).

In the abyssal control volume, the aTTD is characterized by an old water mass age, and a fraction of the trajectories do not reach the surface within the integration period of 1000 years. The location of this particular control volume is the farthest downstream of the

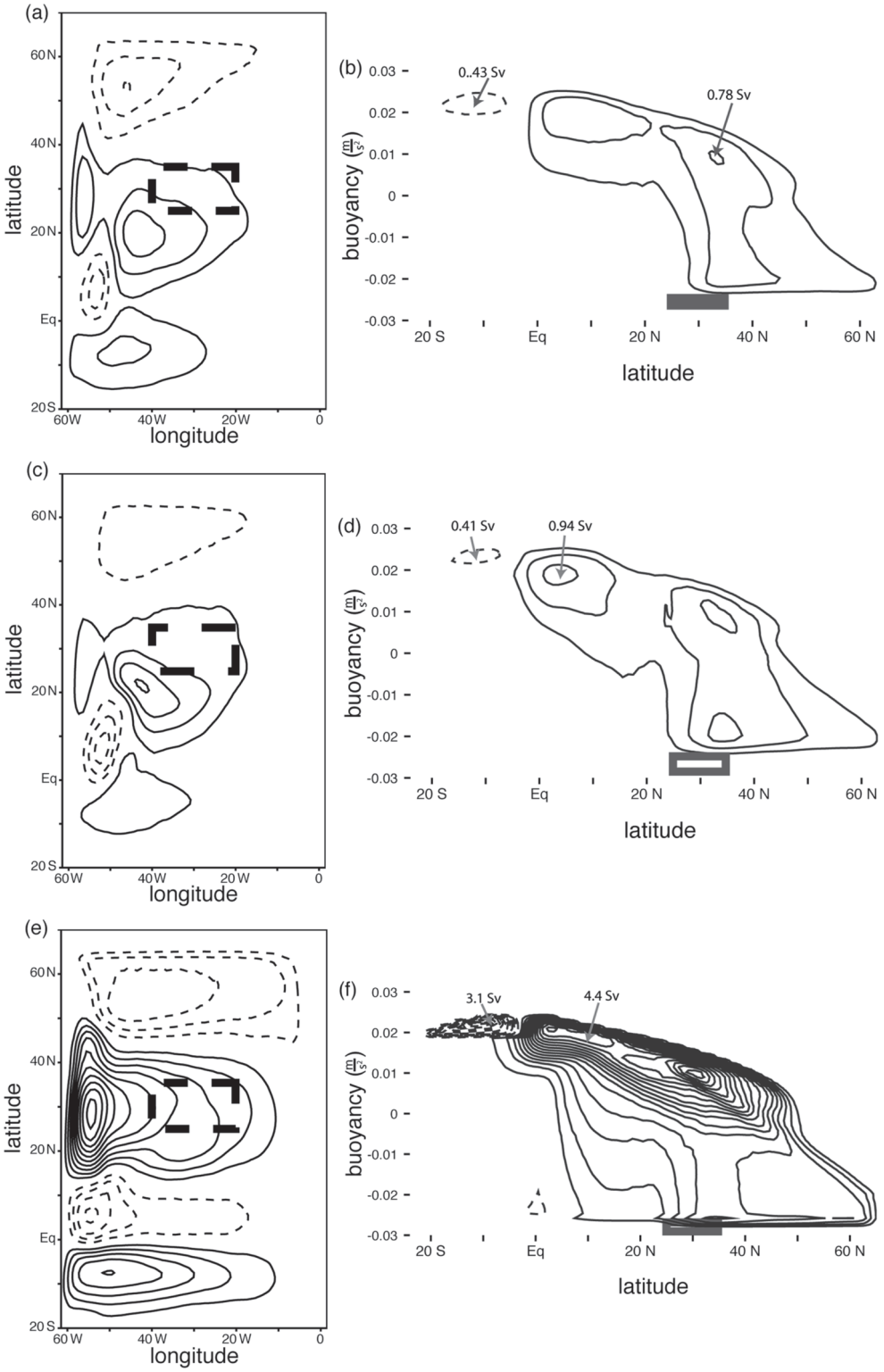

FIG. 15. (a) Barotropic and (b) baroclinic Lagrangian streamfunctions for the CM run. (c),(d) As in (a),(b) but for the FM run; (e),(f) as in (a),(b) but for the HM run. These plots are generated from the control volume spanning 25°–35°N, 40°–20°W [dashed black box in (a)] and 1900–2100 m in depth. The equivalent span in buoyancy (calculated from the zonally integrated buoyancy averaged over the final 10 yr) is demarcated by the gray box in (b). The contour interval is 0.25 Sv.

abyssal circulation, as illustrated by Stommel and Arons (1960). The HM run exhibits the oldest mean age of the all runs in the abyssal ocean because of the lack of diapycnal diffusion in the abyss and the weak ventilation of the deep waters, suggesting that the maintenance of vigorous deep overturning circulation requires diapycnal diffusion at deeper depth levels.

b. *Caveats, limitations, and issues for future study*

The goal of this study is to examine and evaluate the response of the meridional overturning circulation and water mass ages to the highly localized mixing by taking full advantage of the Lagrangian formulation of the model. The LOM is relatively new and is in active development; thus, we have focused on this highly idealized experiment and caution is required when interpreting its relevance to more realistic numerical experiments and to the real ocean.

Here we have chosen to focus on some key physical processes that drive the overturning circulation in an idealized ocean basin. Also, we present a clear and transparent explanation of the sensitivities to the highly localized mixing. Despite these simplifications, aTTD and the associated Lagrangian streamfunctions have effectively demonstrated that water mass trajectories are sensitive to the patterns and magnitudes of the diapycnal diffusion.

c. *Implications for ocean circulation and biogeochemistry modeling*

Diverse applications are possible with the future development of LOM, and one such application is to exploit the explicit control of tracer diffusion in the area of ocean circulation modeling and biogeochemical cycles. The spatial and temporal distributions of diapycnal mixing and its impacts on large-scale ocean circulation are not fully understood nor adequately quantified. This work is a step toward understanding this question, using a highly idealized setting. Inclusion of a zonally reentrant channel may change the behavior of the meridional overturning circulation due to the dynamics of the circumpolar current (Toggweiler and Samuels 1995; Marshall and Radko 2003; Cessi et al. 2006) and is left for future study.

The application to ocean biogeochemical modeling could be fruitful because some gas tracers such as the noble gases are highly sensitive to diapycnal mixing (Henning et al. 2006; Ito and Deutsch 2006). Furthermore, the computational burden for additional tracers is very small because the physical trajectory of the water parcel is already calculated and there is no need to recalculate this transport for additional tracers. The only additional calculations for other tracers are parameterizations of biological sources and sinks.

In this study we have developed aTTD as a new approach for evaluating the water mass ages and the ventilation pathways. It is our hope that these new diagnostics will contribute toward a better understanding of the interplay between physical transport and biological sources and sinks and its control over tracer distributions and fluxes.

Acknowledgments. This research is supported by DOE Cooperative Agreement DE-FC02-01ER63163 with Colorado State University. TI is thankful for the support from the NSF Physical and Chemical Oceanography Program (OCE-0647979) and the NASA Ocean Biology and Biogeochemistry Program (NNX08AL72G). We also wish to thank the two anonymous reviewers, whose comments greatly enhanced the quality of this manuscript.

REFERENCES

Blanke, B., M. Arhan, G. Madec, and S. Roche, 1999: Warm water paths in the equatorial Atlantic as diagnosed with a general circulation model. *J. Phys. Oceanogr.,* **29,** 2753–2768.

Bryan, F., 1987: Parameter sensitivity of primitive equation ocean general circulation models. *J. Phys. Oceanogr.,* **17,** 970–985.

Cessi, P., W. R. Young, and J. A. Polton, 2006: Control of large-scale heat transport by small-scale mixing. *J. Phys. Oceanogr.,* **36,** 1877–1894.

Colin de Verdière, A., 1988: Buoyancy driven planetary flows. *J. Mar. Res.,* **46,** 215–265.

Döös, K., 1995: Inter-ocean exchange of water masses. *J. Geophys. Res.,* **100,** 13 499–13 514.

——, and A. Engqvist, 2007: Assessment of water exchange between a discharge region and the open sea—A comparison of different methodological concepts. *Estuarine Coastal Shelf Sci.,* **74,** 709–721.

——, J. Nycander, and A. C. Coward, 2008: Lagrangian decomposition of the Deacon Cell. *J. Geophys. Res.,* **113,** C07028, doi:10.1029/2007JC004351.

Emanuel, K. A., 1988: The maximum intensity of hurricanes. *J. Atmos. Sci.,* **45,** 1143–1155.

Endoh, T., and T. Hibiya, 2007: Meridional overturning circulation of the deep Pacific estimated assuming the vertical advective-diffusive balance. *Geophys. Res. Lett.,* **34,** L13602, doi:10.1029/2007GL030027.

Garrett, C., 2003: Internal tides and ocean mixing. *Science,* **301,** 1858–1859.

Griffies, S. M., R. C. Pacanowski, and R. W. Hallberg, 2000: Spurious diapycnal mixing associated with advection in a *z*-coordinate model. *Mon. Wea. Rev.,* **128,** 538–564.

Haertel, P. T., and D. A. Randall, 2002: Can a pile of slippery sacks behave like an ocean? *Mon. Wea. Rev.,* **130,** 2975–2988.

——, ——, and T. G. Jensen, 2004: Simulating upwelling in a large lake using slippery sacks. *Mon. Wea. Rev.,* **132,** 66–77.

——, L. P. Van Roekel, and T. G. Jensen, 2009: Constructing an idealized model of the North Atlantic Ocean using slippery sacks. *Ocean Modell.,* **27,** 143–159, doi:10.1016/j.ocemod.2008.12.003.

Harper, S., 2000: Thermocline ventilation and pathways of tropical–subtropical water mass exchange. *Tellus,* **52A,** 330–345.

Hasumi, H., and N. Suginohara, 1999: Effects of locally enhanced vertical diffusivity over rough bathymetry on the World Ocean circulation. *J. Geophys. Res.,* **104** (C10), 23 367–23 374.

Henning, C. C., D. Archer, and I. Fung, 2006: Argon as a tracer of cross-isopycnal mixing in the thermocline. *J. Phys. Oceanogr.,* **36,** 2090–2105.

Hibiya, T., M. Nagasawa, and Y. Niwa, 2006: Global mapping of diapycnal diffusivity in the deep ocean based on the results of expendable current profiler (XCP) surveys. *Geophys. Res. Lett.,* **33,** L03611, doi:10.1029/2005GL025218.

Holzer, M., and T. M. Hall, 2000: Transit-time and tracer-age distributions in geophysical flows. *J. Atmos. Sci.,* **57,** 3539–3558.

Hu, D., 1996: On the sensitivity of thermocline depth and meridional heat transport to vertical diffusivity in OGCMs. *J. Phys. Oceanogr.,* **26,** 1480–1494.

Huang, R. X., and R. L. Chou, 1994: Parameter sensitivity study of the saline circulation. *Climate Dyn.,* **9,** 391–409.

Ito, T., and M. J. Follows, 2003: Upper ocean control on the solubility pump of CO_2. *J. Mar. Res.,* **61,** 465–489.

——, and C. Deutsch, 2006: Understanding the saturation state of argon in the thermocline: The role of air–sea gas exchange and diapycnal mixing. *Global Biogeochem. Cycles,* **20,** GB3019, doi:10.1029/2005GB002655.

Jensen, T. G., 1996: Artificial retardation of barotropic waves in layered ocean models. *Mon. Wea. Rev.,* **124,** 1272–1283.

——, 2001: Application of the GWR method to the tropical oceans. *Mon. Wea. Rev.,* **129,** 470–484.

——, 2003: Barotropic mode errors in an Indian Ocean model associated with the GWR method. *Global Planet. Change,* **37,** 3–20.

Kamenkovich, I. V., and P. J. Goodman, 2001: The dependence of AABW transport in the Atlantic on vertical diffusivity. *Geophys. Res. Lett.,* **28,** 345–346.

Korty, R. L., K. A. Emanuel, and J. R. Scott, 2008: Tropical cyclone-induced upper-ocean mixing and climate: Application to equable climates. *J. Climate,* **21,** 638–654.

Large, W., J. McWilliams, and S. Doney, 1994: Oceanic vertical mixing: A review and a model wih nonlocal boundary layer parameterization. *Rev. Geophys.,* **32,** 363–403.

Ledwell, J. R., A. J. Watson, and C. S. Law, 1993: Evidence for slow mixing across the pycnocline from an open-ocean tracer-release experiment. *Nature,* **364,** 701–703.

Lineikin, P. S., 1955: On the determination of the thickness of the baroclinic layer in the sea. *Dokl. Akad. Nauk. SSSR,* **101,** 461–464.

Luyten, J. R., J. Pedlosky, and H. Stommel, 1983: The ventilated thermocline. *J. Phys. Oceanogr.,* **13,** 292–309.

Marotzke, J., 1997: Boundary mixing and the dynamics of three-dimensional thermohaline circulations. *J. Phys. Oceanogr.,* **27,** 1713–1728.

Marshall, J., and T. Radko, 2003: Residual-mean solutions for the Antarctic Circumpolar Current and its associated overturning circulation. *J. Phys. Oceanogr.,* **33,** 2341–2354.

Munk, W. H., 1966: Abyssal recipes. *Deep-Sea Res.,* **13,** 707–730.

——, and C. Wunsch, 1998: Abyssal recipes II: Energetics of tidal and wind mixing. *Deep-Sea Res. I,* **45,** 1977–2010.

Ozgökmen, T. M., A. Griffa, A. J. Mariano, and L. I. Piterbarg, 2000: On the predictability of Lagrangian trajectories in the ocean. *J. Atmos. Oceanic Technol.,* **17,** 366–383.

Park, Y.-G., and K. Bryan, 2000: Comparison of thermally driven circulations from a depth-coordinate model and an isopycnal-layer model. Part I: Scaling-law sensitivity to vertical diffusivity. *J. Phys. Oceanogr.,* **30,** 590–605.

Polzin, K. L., J. M. Toole, J. R. Ledwell, and R. W. Schmitt, 1997: Spatial variability of turbulent mixing in the abyssal ocean. *Science,* **276,** 93–96.

Robinson, A., and H. Stommel, 1959: The oceanic thermocline and the associated thermohaline circulation. *Tellus,* **11,** 295–308.

Samelson, R. M., 1998: Large-scale circulation with locally enhanced vertical mixing. *J. Phys. Oceanogr.,* **28,** 712–726.

——, and G. K. Vallis, 1997: Large-scale circulation with small diapycnal diffusion: The two-thermocline limit. *J. Mar. Res.,* **55,** 223–275.

Schmitt, R. W., J. R. Ledwell, E. T. Montgomery, K. L. Polzin, and J. M. Toole, 2005: Enhanced diapycnal mixing by salt fingers in the thermocline of the tropical Atlantic. *Science,* **308,** 685–688.

Scott, J. R., and J. Marotzke, 2002: The location of diapycnal mixing and the meridional overturning circulation. *J. Phys. Oceanogr.,* **32,** 3578–3595.

Sriver, R. L., and M. Huber, 2007: Observational evidence for an ocean heat pump induced by tropical cyclones. *Nature,* **447,** 577–580.

Stommel, H., and A. B. Arons, 1960: On the abyssal circulation of the world ocean. I. Stationary planetary flow patterns on a sphere. *Deep-Sea Res.,* **6,** 140–154.

Toggweiler, J. R., and B. Samuels, 1995: Effect of Drake Passage on the global thermohaline circulation. *Deep-Sea Res. I,* **42,** 477–500.

Welander, P., 1986: Thermohaline effects in the ocean circulation and related simple models. *Large-Scale Transport Processes in Oceans and Atmosphere,* J. Willebrand and D. L. T. Anderson, Eds., D. Reidel, 163–200.

Wunsch, C., and R. Ferrari, 2004: Vertical mixing, energy and the general circulation of the oceans. *Annu. Rev. Fluid Mech.,* **36,** 281–314.

Zhang, J. B., R. W. Schmidt, and R. X. Huang, 1999: The relative influence of diapycnal mixing and hydrologic forcing on the stability of the thermohaline circulation. *J. Phys. Oceanogr.,* **29,** 1096–1108.